Hindawi
Complexity
Volume 2020, Article ID 9371327, 9 pages
https://doi.org/10.1155/2020/9371327

Research Article

Structured H_∞ Control of an Electric Power Steering System

Hongbo Zhou,[1] **Aiping Pang**,[1] **Jing Yang**,[1] **and Zhen He**[2]

[1]*College of Electrical Engineering, Guizhou University, Guiyang, CO 550025, China*
[2]*School of Astronautics, Harbin Institute of Technology, Harbin 150000, China*

Correspondence should be addressed to Aiping Pang; 417524788@qq.com

Received 8 May 2020; Revised 27 May 2020; Accepted 9 June 2020; Published 25 July 2020

Guest Editor: Jing Na

Copyright © 2020 Hongbo Zhou et al. This is an open access article distributed under the Creative Commons Attribution License, which permits unrestricted use, distribution, and reproduction in any medium, provided the original work is properly cited.

Electric power steering (EPS) systems are prone to oscillations because of a very small phase angle margin, so a stable controller is required to increase the stability margin. In addition, the EPS system has parameter disturbances in the gain of the torque map under different conditions, which requires a certain degree of robustness in the control design. This paper synthesizes the multidimensional performance requirements considering the stability margin, robustness, and bandwidth of the system to form an H_∞ optimization matrix with multidimensional performance output in using the structured H_∞ control design. The structured H_∞ controller not only retains the characteristics of traditional H_∞ controllers with excellent robust performance and high stability margin but also has a lower order, which can be better applied in practice. Based on the performance requirements of the system and practical implementation, the structured H_∞ controllers with different orders were designed, and the feasibility of the structured controller was confirmed through comparison and theoretical analysis.

1. Introduction

The electric power steering (EPS) system is a steering system supported by motors, which offers drivers lighter steering experience. Comparing with hydraulic power steering (HPS), EPS has many advantages including better fuel efficiency, smaller size, and the feeling of steering easily, in addition, the capability to combine other electric control systems in the car with itself, so most cars are equipped with an EPS system [1]. When the driver turns the steering wheel, the torque sensor detects the steering angle and torque and sends a voltage signal to the electronic control unit. The electronic control unit sends instructions to the motor control unit based on the torque voltage signal, direction of rotation, and speed signal detected by the torque sensor, so that the motor outputs the steering booster torque of the corresponding size and torque.

Although the EPS system has many advantages, designing a suitable controller for EPS is a challenging problem for many reasons. Torque map is the main component of the EPS controller. The torque map is a gain function between the measured torque from the steering wheel and the assist torque provided by the motor. It determines how much steering torque the motor assists. The shape of the torque map determines the driver's driving feeling [2]. Generally, since the torque required to steer is maximum when parking, the slope of the torque map is steepest at zero speed, and then decreases as the speed increases. When driving at low speed, the high gain of the controller and the nonlinearity of the torque map cause the instability and vibration [3–5]. Due to the dynamic uncertainty (unmodeled dynamic characteristics) and parameter uncertainty of the EPS system, the controller must be robust. Even for the same type of vehicle, the system parameters of each vehicle will be different, so the tuning of the parameters also faces huge challenges [6]. In addition, the steering system is in an extremely sensitive state to interact with the driver's hand, so a good controller design should eliminate unwanted vibrations.

There are many researches on the EPS system controller and various EPS controllers are proposed to ensure the system stability. In [7], the authors analyze the stability conditions based on the EPS model and use a structured structure compensator to realize the system stability and torque vibration minimization. In [8], the authors use frequency weighted damping compensator to improve the phase margin of the system, improving the stability of the system, but the phase margin is limited. In [9], the authors use an integral sliding mode controller to generate the power

torque so that the system can achieve stability and improve the damping characteristics of the system. In [10], the authors analyze the stability of a system with approximately linear torque diagrams and nonlinear torque diagrams, propose criteria for designing a stable compensator, and give lead-lag compensators of different orders. The lead-lag compensator with different parameters is applied together with the torque map for vehicle experiments.

However, the previous control design has some limitations. Firstly, most researches approximate the nonlinear torque diagram as a simple linear gain without analyzing the influence of nonlinearity on the stability of the system. In addition, the main concern of these designs is whether the control system is stable or not, without considering the robustness and control performance comprehensively. H_∞ control can consider many aspects of the design requirements, such as robust stability, system bandwidth requirements, output performance, and so on. The study [11] gives a H_∞ controller that enhances the close-loop robustness of the system and improves the steering comfort, but its limitation is that the order of the H_∞ controller is too high to realize in practical application. In recent years, Apkarian et al. proposed a new structured H_∞ comprehensive control method [12, 13]. Compared with the traditional H_∞ control method, the advantage of structured H_∞ control is that the structure or order of the controller can be set in advance. In other words, the controller meets the performance requirements and simultaneously has a relatively simple structure.

Aiming at the stability and comprehensive performance of the EPS system, this paper adopts a structured H_∞ control method and gives the controller design and parameter optimization results under a given torque diagram. Taking a cylindrical EPS system as an example, we analyze the system performance under two sources of instability with large gain at low speed and nonlinearity caused by torque diagram and design a structured H_∞ controller according to the system performance requirements. First, considering that the high order of the traditional H_∞ controller is not conducive to the actual production, we determined the order and structure of the controller and designed the controller structure of 2nd order to 4th order. Then, we selected appropriate weight functions according to the performance requirements of the system. Finally, we obtained the optimal parameters that met the system performance requirements through simulation calculations and verified the theoretical design through simulation analysis.

2. EPS System Model

According to the different positions of power supply, the EPS system can be divided into three types: steering column type, pinion type, and rack type. In this paper, we will take the column EPS system (C-EPS) as an example. It is mainly composed of four parts: steering wheel, column, motor, and rack. The steering wheel and steering column are connected by a torque sensor including an elastic torsion bar, and the motor and rack are respectively connected to the steering column by a reduction mechanism (in this case, it is a worm reduction mechanism) and a pinion. The dynamic model is shown in Figure 1, and the meaning of each variable and parameter throughout this paper is shown in the figures and is defined in Table 1.

The equations of motion of each part of the system are listed as in the following equations:

$$J_1\ddot{\theta}_1 + C_1\dot{\theta}_1 + K(\theta_1 - \theta_2) = \tau_h, \tag{1}$$

$$J_c\ddot{\theta}_2 + C_c\dot{\theta}_2 + K(\theta_2 - \theta_1) = \tau_{\text{gear}} - \tau_{\text{pinion}}, \tag{2}$$

$$J_m\ddot{\theta}_m + C_m\dot{\theta}_m = \frac{\tau_m - \tau_{\text{gear}}}{N}, \tag{3}$$

$$M_r\ddot{x}_r + C_r\dot{x}_r = \frac{\tau_{\text{pinion}}}{r_p} - F_{\text{load}}. \tag{4}$$

The gear ratio of rack, pinion, and worm gear are shown in the following equation:

$$\begin{aligned} r_p\theta_2 &= x_r, \\ N\theta_2 &= \theta_m. \end{aligned} \tag{5}$$

Equations (2)–(4) can be simplified to a lumped mass equation as shown in the following equation:

$$J_2\ddot{\theta}_2 + C_2\dot{\theta}_2 + K(\theta_2 - \theta_1) = \tau_a - \tau_l, \tag{6}$$

where equivalent moment of inertia J_2, equivalent damping coefficient C_2, equivalent boost torque τ_a , and equivalent load torque τ_l are determined in the following equation:

$$\left.\begin{aligned} J_2 &= J_c + N^2J_m + r_pM_r \\ C_2 &= C_c + N^2C_m + r_pC_r \\ \tau_a &= N\tau_m \\ \tau_1 &= r_pF_{\text{load}} \end{aligned}\right\}. \tag{7}$$

The system block diagram of the EPS system is shown in Figure 2, which describes the relationship between the system's external input (steering wheel torque and equivalent load torque) and the system state variables (steering wheel angle and steering column angle).

As shown in Figure 2, h is the EPS controller consisting of a torque map and a compensation controller. τ_s is the measure torque on the torque sensor, and $\tau_{a,\text{ref}}$ is the reference value of the boost torque calculated by the controller, listed as in the following equations:

$$\tau_s = K(\theta_1 - \theta_2), \tag{8}$$

$$\tau_{a,\text{ref}} = h \cdot \tau_s. \tag{9}$$

The transfer function from steering wheel torque to output angle θ_1 is as follows:

$$G_w(s) = \frac{1}{J_1s^2 + C_1s}. \tag{10}$$

The transfer function from the steering column moment to output angle θ_2 is as follows:

$$G_c(s) = \frac{1}{J_2s^2 + C_2s}. \tag{11}$$

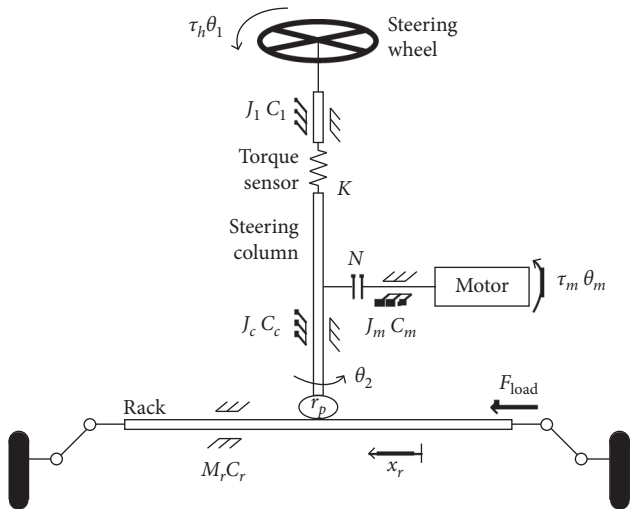

Figure 1: EPS system model.

Table 1: Parameters and variables.

Notation	Description
J_1	Moment of inertia of steering wheel
C_1	Damping coefficient of the steering wheel
K	Torsional stiffness of torque sensor
J_c	Moment of inertia of column
C_c	Damping coefficient of column
J_m	Moment of inertia of motor
C_m	Damping coefficient of motor
θ_1	Steering wheel angle
θ_2	Column angle
θ_m	Motor angle
τ_h	Driver torque
τ_m	Motor torque
τ_{pinion}	Pinon torque
τ_{gear}	Gear torque
N	Gear ratio
M_r	Mass of rack
C_r	Damping coefficient of rack
x_r	Rack displacement
r_p	Pinion radius
F_{load}	Load force of rack from tire

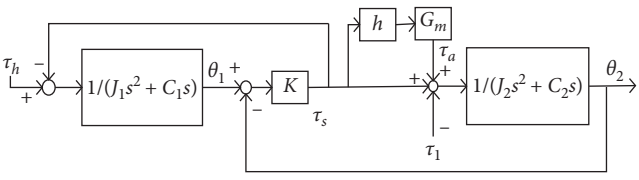

Figure 2: Block diagram of the EPS system.

The mathematical model of the engine in the system can be expressed as low-pass filter with a cutoff frequency of ω_m as follows:

$$G_m(s) = \frac{\tau_a}{\tau_{a,\text{ref}}} = \frac{\omega_m}{s + \omega_m}. \tag{12}$$

The parameters adopted for the EPS system in literature [7] are shown in Table 2:

Table 2: Value of the parameters of EPS.

Parameters	Value
K	143.24
J_1 (kg·m^2)	0.044
C_1 (Nm·s/rad)	0.25
J_2 (kg·m^2)	0.11
C_2 (Nm·s/rad)	1.35
ω_m (rad/s)	200π

3. Structured H_∞ Controller Design

In this case, the control design of the EPS system involves multiple control objectives, so the design of the structured H_∞ is adopted. It not only retains the synthesis of traditional H_∞ design but also can be weighted for each performance requirement to form a diagonal matrix with multidimensional performance output for performance synthesis optimization [14, 15].

A complete structured H_∞ control design can be generally divided into three steps: first, the performance requirements of the system should be analyzed according to the control objectives; then, the appropriate weighting functions should be selected according to the specific performance requirements and optimization objectives, and multiple weighting performance requirements should be formed into a diagonal optimization matrix; finally, a structured control with adjustable parameters should be determined in the light of the actual needs and design objectives [16–19]. The structured H_∞ controller satisfying the comprehensive performance requirements is obtained by solving the optimal controller parameters.

3.1. Controller Structure. The control structure of the system is shown in Figure 3. In the EPS system, the driver inputs the steering angle signal θ_1 from the steering wheel, and the control center gets the steering column measurement torque τ_s from the torque sensor, and inputs it into the controller to obtain the desired torque boosting torque $\tau_{a,\text{ref}}$, where the value of τ_a^* before passing through the stability controller is given by the following equation:

$$\tau_a^* = \begin{cases} 0, & 0 \le \tau_s \le \tau_{s0}, \\ K_v v_{\text{car}}(\tau_s - \tau_{s0}), & \tau_{s0} < \tau_s. \end{cases} \tag{13}$$

The torque map has a dead zone below τ_{s0} to prevent the system from being too sensitive to the driver's small-angle steering, especially at high speeds. It is the dead zone that causes the nonlinearity of the system. In the parking state, the driver needs a larger assist torque, while at high speed, it needs less assist torque, so K_v decreases as the vehicle speed increases. Compared to the torque map in Figure 3, the torque map applied to a conventional vehicle is a smoother curve, but to simplify the analysis, we use a proportional function with a dead zone. Generally, $K_v = 35$ in the moment diagram.

EPS controllers also require some type of stability compensator due to the instability of the system caused by the high gain and nonlinearity of the torque map at low

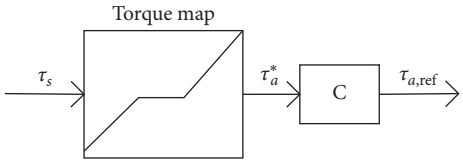

Figure 3: Controller structure of the EPS.

speeds. We use a structured H_∞ controller as a stability controller behind the torque map, which provides the controller with dynamic characteristics while ensuring stability and robustness and suppressing the vibration of the entire EPS system. The structured H_∞ compensator is shown in the following equation:

$$C = \prod_{i=1}^{n} C_i(s) = \prod_{i=1}^{n} \frac{s/b_i + 1}{s/a_i + 1}, \quad n = 1, 2, \ldots, L, \tag{14}$$

where $a_i b_i$ are parameters to be optimized and n in subscript indicates the order of the controller.

3.2. Stability Analysis and Weight Function Choice. By the analysis, the performance requirements of the control design are as follows: stability margin, robust stability, and system bandwidth.

3.2.1. Stability Margin. From the system models (1)–(12), the phase margin is only $\gamma = 8.54^\circ$, and the stability margin of the system is too small. In order to improve driving comfort, the first performance requirement of the controller design is stability margin.

T_1 is the transfer function from r to e shown in Figure 4 where r is the disturbance signal and e is an error signal. The stability of the system is the distance of the transfer function from the critical stability point. It is also the upper limit of the gain toward the sensitivity function [19, 20]. It required the following:

$$\left\| W_1(s) T_1(s) \right\|_\infty \le \gamma_1. \tag{15}$$

In formula (15), γ_1 is the norm index and $W_1(s)$ is the weighting function. The upper limit of the stability margin is given as 0.8, $W_1(s) = 0.8$.

3.2.2. Bandwidth Requirement. Except for the stability, it is also necessary to consider the appropriate bandwidth of the system. T_2 represents the transfer function from r to τ_s. The system bandwidth requirement is as follows:

$$\left\| W_2(s) T_2(s) \right\|_\infty \le \gamma_2. \tag{16}$$

To limit the bandwidth of the system, the weighted function $W_2(s)$ is selected as the following high-pass filtering form:

$$W_2(s) = \frac{2s}{s + 1200}. \tag{17}$$

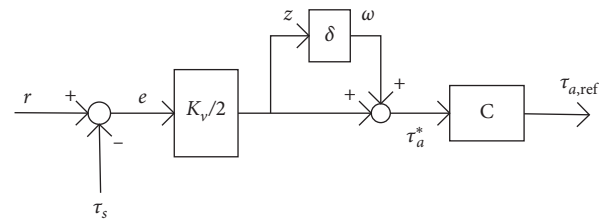

Figure 4: Controller structure with uncertainty.

3.2.3. Robust Stability. Considering the uncertainty of the power moment ratio K_v of EPS system due to different external conditions and the nonlinearity of the dead zone, τ_a^* is expressed as follows:

$$\tau_a^* = \tau_s \left(\frac{K_v}{2} + \frac{K_v}{2} \delta \right), \quad |\delta| \le 1, \tag{18}$$

where δ is the perturbation parameter.

The control structure diagram of the system according to equation (18) is shown in Figure 4.

According to the principle of minimum gain, the robust stability of the system needs to satisfy the condition of the following equation:

$$\left\| T_{z\omega} \right\|_\infty < 1. \tag{19}$$

Therefore, the second performance requirement of the system is robust stability. T_3 is the transfer function from ω to z. The requirement of the system for robust stability is as follows:

$$\left\| W_3(s) T_3(s) \right\|_\infty \le \gamma_3, \tag{20}$$

where the weighting function is $W_3(s) = 1$.

For the H_∞ control optimization problem where the order has been fixed and has selected the weighting function, the control performance requirements of the EPS system are comprehensively considered and the minimum value satisfying (21) is obtained by optimizing the adjustable parameters a_i and b_i:

$$\begin{aligned} &\|H\|_\infty \le \min\{\gamma_i\}, \\ &H = \operatorname{diag}\left(W_1 T_1 \;\; W_2 T_2 \;\; W_3 T_3 \right). \end{aligned} \tag{21}$$

At this time, the adjustable parameters obtained are the optimal parameters of the system controller.

When the optimal parameters in the structured H_∞ controller are obtained, T_1, T_2, and T_3 in (21) are expressed as the following linear fraction form P_1, P_2, and P_3 in (22), where the parameters in the structured controller (C) are extracted for optimization by the method of linear fractional transformation (LFT) [21–24]:

$$\begin{cases} T_1 = F_l\left(P_1 \;\; C \right), \\ T_2 = F_l\left(P_2 \;\; C \right), \\ T_3 = F_l\left(P_3 \;\; C \right). \end{cases} \tag{22}$$

3.3. Controller Design Results. In the parking state which means $h = K_v$, the phase margin without compensator is only $\gamma = 8.54^\circ$, which is shown in Figure 5. We decided to use at

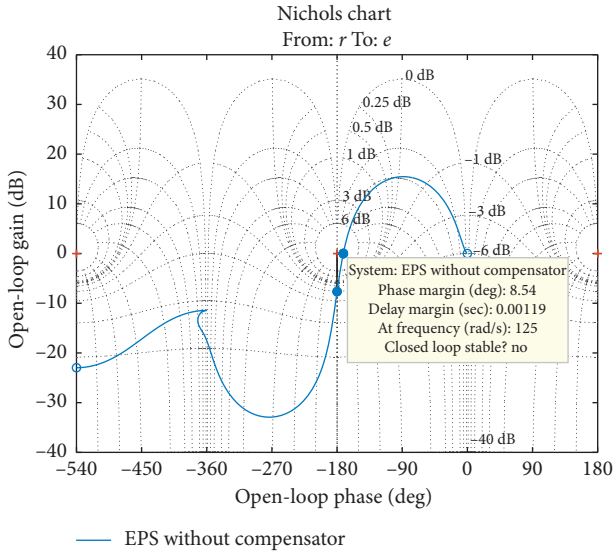

Figure 5: Nichols chart of EPS without compensator.

least a second-order compensator as a controller in order to ensure the stability margin (phase margin) is more than 45°.

According to the system performance requirements and stability analysis, we designed the structured compensator of different orders as the controller in turn. As shown in (14), when $n=2$, the controller is a second-order compensator (controller 1); when $n=3$, the controller is a third-order compensator (controller 2); when $n=4$, the controller is a fourth-order compensator (controller 3). The parameters used in structured H_∞ controllers and index norms of each controller are shown as in Table 3.

Under normal circumstances, we assume that the system can achieve good performance when the γ value is less than 1. As the controller order increases, the γ value we get will become smaller and smaller. The value of γ of the second-order controller still exceeds 1, and the value of γ is already less than 1 when the order of controller is increased to the third order. Although the γ value is still decreasing when the order increased to the fourth order, the degree of reduction is not obvious. Therefore, we think it is not necessary to increase the controller order, so we have only designed controllers with 2–4 orders.

4. Simulation Analysis

The simulation environment is built using Simulink. It consists of steering machinery, controller, motor, and road disturbances. In the parking state, the road disturbance is shown in the following equation:

$$\tau_{l,k} = K_{\text{park}}\left(\theta_{2,k} - \theta_{t,k}\right),$$
$$\theta_{t,k} = \begin{cases} \theta_{2,k} - \theta_{\max}, & \theta_{2,k} - \theta_{t,k-1} > \theta_{\max}, \\ \theta_{2,k} + \theta_{\max}, & \theta_{2,k} - \theta_{t,k-1} > -\theta_{\max}, \\ \theta_{t,k-1}, & \text{otherwise.} \end{cases} \tag{23}$$

Table 3: Controllers design parameter.

Controller	1	2	3
a_1	537	1039	1019
b_1	8	5.39	2.22
a_2	2	403	0.5
b_2	40.2	127	146
a_3	—	2	18.3
b_3	—	135	168
a_4	—	—	513
b_4	—	—	14.6
γ	1.4340	1.0768	0.9621

The symbol "—" indicates that the value is the default value.

In the driving state, the road disturbance is proportional to the steering angle as in the following equation:

$$\tau_{l,k} = K_{\text{drive}}\theta_{2,k}, \tag{24}$$

In the following, we will apply the compensation controllers of different orders (2^{nd}, 3^{rd}, 4^{th} order) obtained previously to simulate the EPS system. We will compare and analyze the performance of the system in terms of stability margin, bandwidth, and robust stability under the action of three controllers, similar to designing a controller.

4.1. Simulation Analysis of Stability Margin. Under the action of different structured H_∞ controllers, the open-loop Nichols diagram of the system is shown in Figure 6. Under the action of controllers with different structures, the stability margin of the system has been greatly improved. With the increase of the order of controller, we find that the stability margin of the sensitivity function can meet the performance requirements of the system, but the difference between different orders is not obvious.

4.2. Simulation Analysis of Bandwidth. Figure 7 shows the Bode diagram under the action of the controller (1, 2, 3), where the full line is the Bode graph of T_2, and the dotted line corresponds to the weighted function W_2. The magnitude of T_2 decreases rapidly before reaching the turning frequency of $1/W_2$. Under the restriction of the weighting function W_2, the overall amplitude of the system is all below the amplitude of $1/W_2$, and all of the controllers meet the bandwidth limitation of the control objective.

The corresponding stability margins are shown in Table 4. For the improvement of the phase margin, the effects of controllers 2 and 3 are almost similar, and the phase angle margin of the system is greatly increased compared to the controller 1. There is no obvious difference between the three controllers for increasing the amplitude margin. As the structured controller order and phase angle margin increase, we can see that the sheer frequency of the system is continuously decreasing.

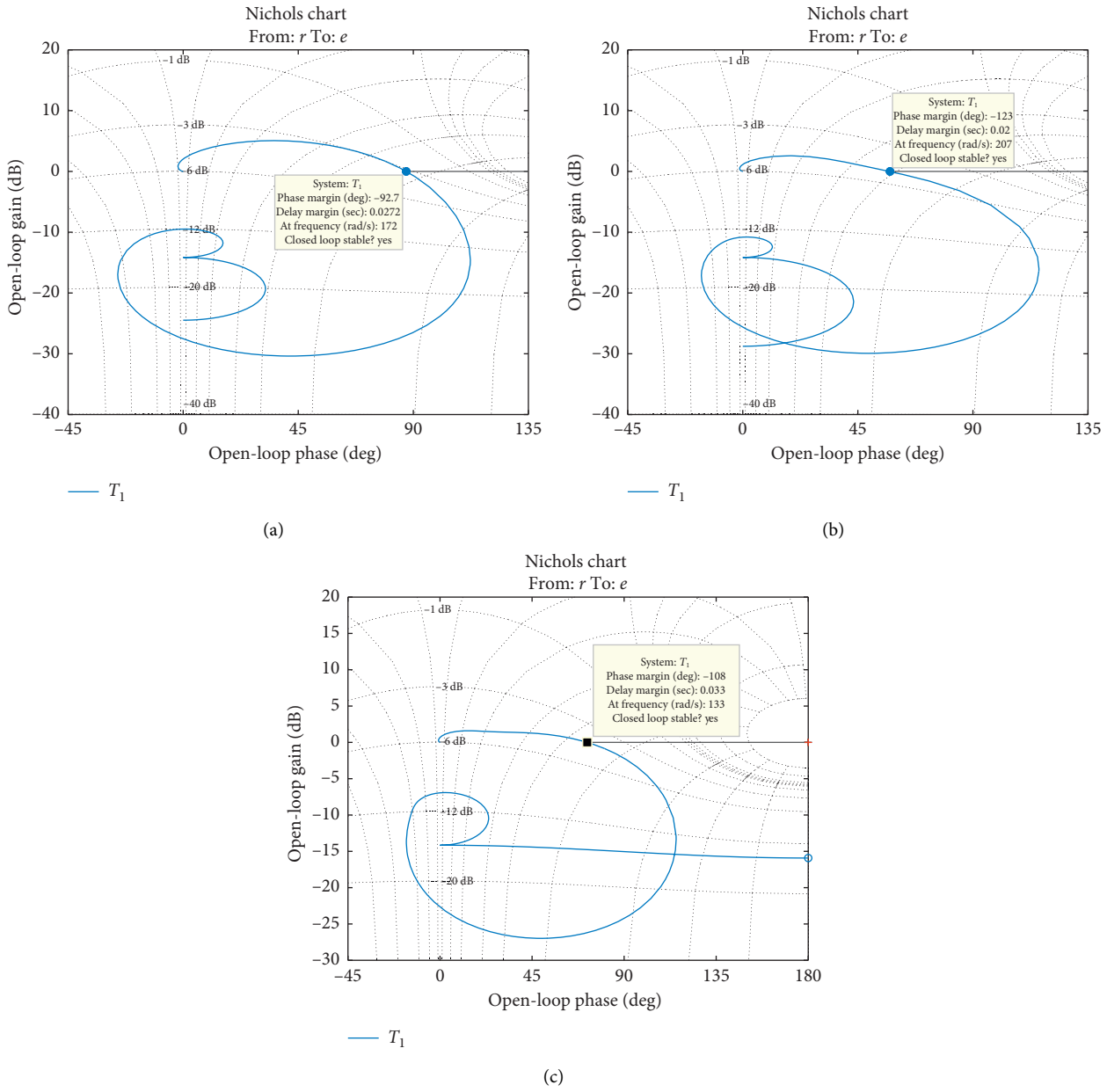

Figure 6: Nichols plots of EPS with (a) controller 1, (b) controller 2, and (c) controller 3.

4.3. Simulation Analysis of Robust Stability. In order to verify the robustness of the designed controllers, the perturbation parameter is given to $\delta = 0.86$, $K_v = 30$, and a sine function with an amplitude of π rad and a frequency of π rad/s is given at the input command of steering angle for simulation. Figure 8 shows the comparison between the sinusoidal input and output measured values τ_s. The dotted line is the sinusoidal input, which is the angle of the steering wheel, and the solid line is the output torque of the steering column. Due to the nonlinearity of the torque graph, we can see that the output steering torque has a significant chattering phenomenon at the dead zone characteristics.

Obviously, all control designs have good robustness and can effectively suppress the oscillations generated by the system. The oscillation amplitude of the system is limited within the 0.7 N · m under controller 1 but 0.2 N · m under controller 3. By comparison, we can conclude that controller 1 is relatively weak in suppressing chattering, while controllers 2 and 3 perform well in eliminating chattering. And as the controller's order increases, its ability to suppress chatter and its robust stability also become more outstanding.

Based on the analysis of the simulation results of the stability margin, bandwidth, and robust stability, the three controllers designed with different orders (2^{nd}–4^{th} order) can satisfy the performance requirements. It is undeniable that with the increase of the controller order, we can conclude that the phase margin, the bandwidth, and the robust stability of

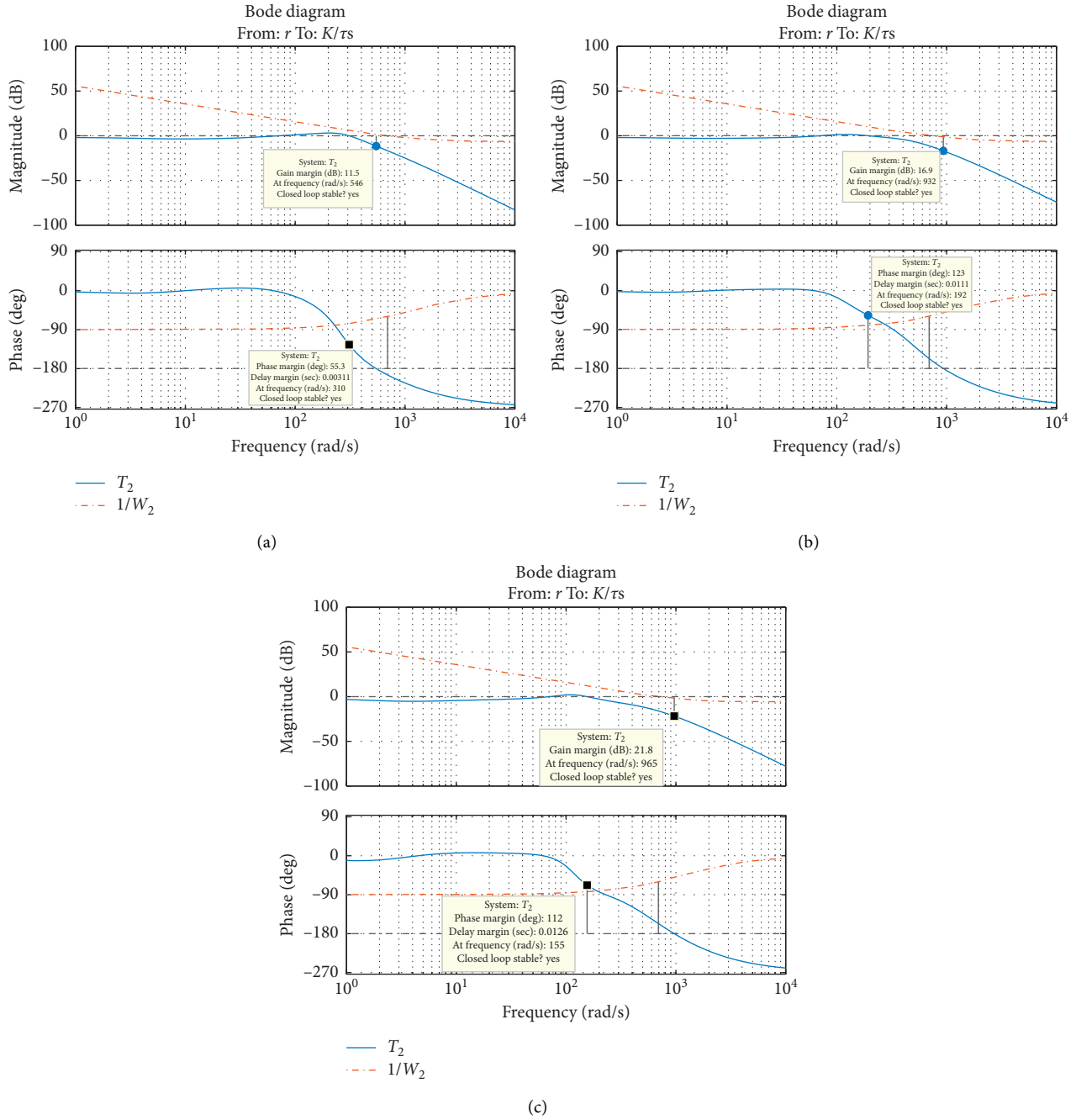

Figure 7: Bode plots of T_2 and $1/W_2$ of (a) controller 1, (b) controller 2, and (c) controller 3.

Table 4: Condition parameters of the controller.

Controller	1	2	3
PM	55.3°	123°	112°
GM	11.5°	16.9 dB	21.8 dB
Cut frequency	310°	192 rad	155 rad

the system have improved significantly. Controller 2 (third-order) has performed very well in all aspects, and controller 3 (fourth-order) is even better in terms of robust stability. Moreover, controllers 2 and 3 are achievable in practical production applications and have engineering application value while meeting the system performance requirements.

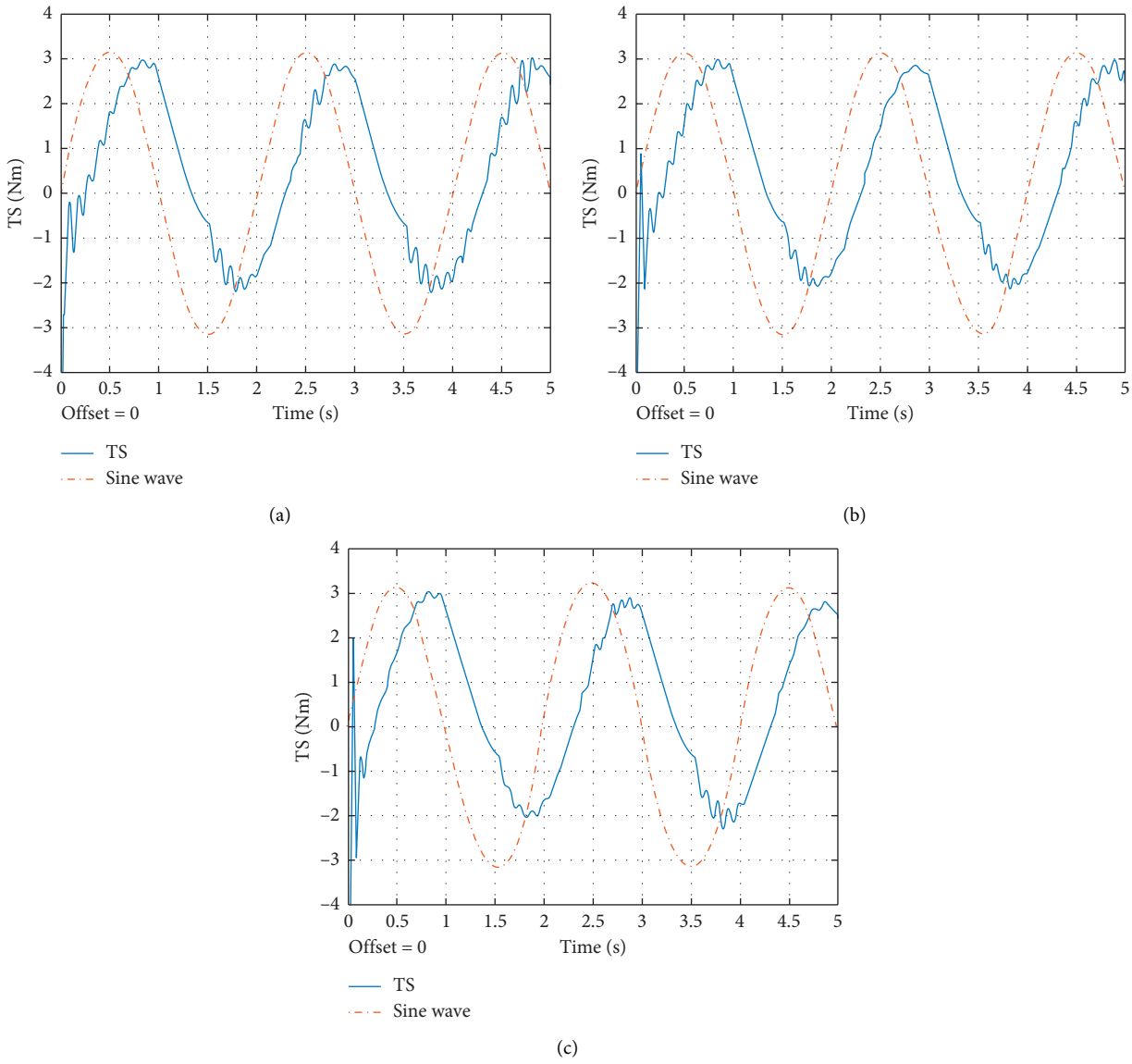

Figure 8: Simulation result of (a) controller 1, (b) controller 2, and (c) controller 3.

5. Conclusion

The low stability margin of the EPS system and the perturbation of parameters in the torque map will cause control problems such as robustness and bandwidth requirements. Based on the H_∞ control method, this paper selects an appropriate weighting function to limit the stability margin and bandwidth of the system by analyzing the system performance requirements. We present a structured H_∞ controller with a higher stability margin, good robustness, and lower order. The simulation results show that the controller designed in this paper has good robustness, can reach the required stability margin, and can suppress the system oscillation within the range of $0.5\,\mathrm{N}\cdot\mathrm{m}$. The design ideas adopted in this paper and the selection of weighting functions can provide some reference for a wide range of control systems.

Data Availability

The data used to support the findings of this study are included within the article. Other data or programs used to support the findings of this study are available from the corresponding author upon request.

Conflicts of Interest

The authors declare that they have no conflicts of interest.

Acknowledgments

This work was supported by the National Natural Science Foundation of China (Nos. 61790562, 61861007 and 61640014), the Guizhou Provincial Science and Technology Foundation (QianHe [2020]1Y273 and [2020]1Y266),

Industrial Project of Guizhou Province (QiankeheZhicheng [2019]2152), Postgraduate Case Library (KCALK201708), and Important Subject of Guizhou Province (QianxueweiHe ZDXK[2015]8).

References

[1] X. Chen, T. Yang, X. Chen, and K. Zhou, "A generic model-based advanced control of electric power-assisted steering systems," *IEEE Transactions on Control Systems Technology*, vol. 16, no. 6, pp. 1289–1300, 2008.

[2] M. H. Lee, S. Ki Ha, J. Y. Choi, and K. S. Yoon, "Improvement of the steering feel of an electric power steering system by torque map modification," *Journal of Mechanical Science and Technology*, vol. 19, no. 3, pp. 792–801, 2005.

[3] J. Na, B. Jing, Y. Huang, G. Gao, and C. Zhang, "Unknown system dynamics estimator for motion control of nonlinear robotic systems," *IEEE Transactions on Industrial Electronics*, vol. 67, no. 5, pp. 3850–3859, 2020.

[4] J. Zhang, G. Xiong, K. Meng, P. Yu, G. Yao, and Z. Dong, "An improved probabilistic load flow simulation method considering correlated stochastic variables," *International Journal of Electrical Power & Energy Systems*, vol. 111, pp. 260–268, 2019.

[5] A. Marouf, M. Djemai, C. Sentouh, and P. Pudlo, "A new control strategy of an electric-power-assisted steering system," *IEEE Transactions on Vehicular Technology*, vol. 61, no. 8, pp. 3574–3589, 2012.

[6] A. T. Zaremba, M. K. Liubakka, and R. M. Stuntz, "Control and steering feel issues the design of an electric power steering system," in *Proceedings of the 1998 American Control Conference*, vol. 1, pp. 36–40, Philadelphia, PA, USA, June 1998.

[7] M. Kurishige, O. Nishihara, and H. Kumamoto, "A new control strategy to reduce steering torque without perceptible vibration for vehicles equipped with electric power steering," *Journal of Vibration and Acoustics*, vol. 132, no. 5, Article ID 054504, 2010.

[8] A. Marouf, C. Sentouh, M. Djemai, and P. Pudlo, "Control of electric power assisted steering system using sliding mode control," in *Proceedings of the 14th International IEEE Conference on Intelligent Transportation Systems (ITSC)*, vol. 10, pp. 107–112, Washington, DC, USA, October 2011.

[9] D. Lee, K. Kyung-Soo, and S. Kim, "Controller design of an electric power steering system," *IEEE Transactions on Control Systems Technology*, vol. 10, no. 1109, pp. 1–8, 2017.

[10] R. Chabaan and L. Y. Wang, "Control of electrical power assist systems: H_∞ design, torque estimation and structural stability," *JSAE Review*, vol. 22, no. 4, pp. 435–444, 2001.

[11] P. Gahinet and P. Apkarian, "Frequency-domain tuning of fixed-structure control systems," in *Proceedings of the UKACC International Conference on Control*, IEEE, Cardiff, UK, pp. 178–183, 2012.

[12] P. Apkarian and D. Noll, "Structured *H*-infinity control of infinite dimensional systems," *International Journal of Robust & Nonlinear Control*, vol. 1, 2017.

[13] G. X. Wang and Z. He, *Applied H_∞ Control*, Harbin Institute of Technology Press, Harbin, China, 2010.

[14] A.-p. Pang, Z. He, M.-h. Zhao, G.-x. Wang, Q.-m. Wu, and Z.-t. Li, "Sum of squares approach for nonlinear H_∞ control," *Complexity*, vol. 2018, Article ID 8325609, 7 pages, 2018.

[15] P. Apkarian, "Tuning controllers against multiple design requirements," in *Proceedings of the American Control Conference*, IEEE, Montreal, Canada, pp. 3888–3893, 2012.

[16] P. Apkarian, M. N. Dao, and D. Noll, "Parametric robust structured control design," *IEEE Transactions on Automatic Control*, vol. 60, no. 7, pp. 1857–1869, 2015.

[17] G. F. Franklin, J. D. Powell, and A. Emami-Naeini, *Feedback Control of Dynamic Systems*, Pearson Education, Upper Saddle River, NJ, USA, 6th edition, 2010.

[18] J. Na, Y. Huang, X. Wu, S.-F. Su, and G. Li, "Adaptive finite-time fuzzy control of nonlinear active suspension systems with input delay," *IEEE Transactions on Cybernetics*, vol. 50, no. 6, pp. 2639–2650, 2020.

[19] P. Apkarian and D. Noll, "Nonsmooth optimization for multidisk H_∞ synthesis," *European Journal of Control*, vol. 12, no. 3, pp. 229–244, 2006.

[20] F. Meng, X. A. Pang, X. C. Dong, C. Han, and X. Sha, "H_∞ optimal performance design of an unstable plant under bode integral constraint," *Complexity*, vol. 2018, Article ID 4942906, 10 pages, 2018.

[21] P. Gahinet and P. Apkarian, "Structured H_∞ synthesis in MATLAB," *IFAC Proceedings Volumes*, vol. 44, no. 1, pp. 1435–1440, 2011.

[22] R. S. D. S. D. Aguiar, P. Apkarian, and D. Noll, "Structured robust control against mixed uncertainty," *IEEE Transactions on Control Systems Technology*, vol. 99, pp. 1–11, 2017.

[23] J. Zhang, L. Fan, Y. Zhang et al., "A probabilistic assessment method for voltage stability considering large scale correlated stochastic variables," *IEEE Access*, vol. 8, pp. 5407–5415, 2020.

[24] P. Gahinet and P. Apkarian, "Decentralized and fixed-structure H_∞ control in MATLAB," in *Proceedings of the IEEE Conference on Decision and Control and European Control Conference*, pp. 8205–8210, Orlando, FL, USA, 2011.